CLIMATOLOGY

Extensive fires in southeastern Siberian permafrost linked to preceding Arctic Oscillation

Jin-Soo Kim[1,2], Jong-Seong Kug[3]*, Su-Jong Jeong[4,5], Hotaek Park[6], Gabriela Schaepman-Strub[7]

Carbon release through boreal fires could considerably accelerate Arctic warming; however, boreal fire occurrence mechanisms and dynamics remain largely unknown. Here, we analyze fire activity and relevant large-scale atmospheric conditions over southeastern Siberia, which has the largest burned area fraction in the circumboreal and high-level carbon emissions due to high-density peatlands. It is found that the annual burned area increased when a positive Arctic Oscillation (AO) takes place in early months of the year, despite peak fire season occurring 1 to 2 months later. A local high-pressure system linked to the AO drives a high-temperature anomaly in late winter, causing premature snowmelt. This causes earlier ground surface exposure and drier ground in spring due to enhanced evaporation, promoting fire spreading. Recently, southeastern Siberia has experienced warming and snow retreat; therefore, southeastern Siberia requires appropriate fire management strategies to prevent massive carbon release and accelerated global warming.

INTRODUCTION

Arctic permafrost has received attention as a potential global warming amplifier. Permafrost zone carbon stocks are estimated to be more than double the atmospheric carbon pool (~750 PgC) (*1*). The large quantities of carbon stored in frozen soils can be released into the atmosphere through ongoing degradation of permafrost resulting from recent Arctic warming (*2*, *3*). In addition to carbon release from thawing permafrost, over the past two decades, boreal fires have released substantial amounts of carbon in boreal North America (60 TgC year^{-1}) and Asia (124 TgC year^{-1}) (*4*). Carbon release by boreal fires can accelerate global and Arctic warming and play a role in positive feedback between accumulation of atmospheric carbon and Arctic warming (*5*, *6*).

Fires in the northern circumpolar region show a distinct spatial distribution that consists of two major regions in Central Asia and southeastern Siberia. The Global Fire Emissions Database version 4.1 with small fires (GFED4.1s) gives an observed burned fraction of more than 10% year^{-1} over the past 20 years in this region (Fig. 1A) (*7*). Central Asia has an extensive burned area, but this is mostly from agricultural fires surrounding the Black Sea (*8*). In contrast, southeastern Siberia (100°–150°E, 45°–55°N), which contains dense boreal forests and peatlands in the permafrost zone, has had substantial forest fires. Although climate phenomena such as the El Niño–Southern Oscillation (ENSO) and Arctic Oscillation (AO) have been reported as affecting fire activity in several key regions through driving atmospheric processes (*9*–*13*), there is still a considerable lack of understanding of fire activity variability, especially in permafrost areas, despite their importance for global climate.

[1]School of GeoSciences, University of Edinburgh, Edinburgh, UK. [2]National Centre for Earth Observation, University of Edinburgh, Edinburgh, UK. [3]Division of Environmental Science and Engineering, Pohang University of Science and Technology (POSTECH), Pohang, South Korea. [4]Department of Environmental Planning, Graduate School of Environmental Studies, Seoul National University, Seoul, South Korea. [5]Institute for Sustainable Development (ISD), Seoul National University, Seoul, South Korea. [6]Institute of Arctic Climate and Environmental Research, Japan Agency for Marine-Earth Science and Technology (JAMSTEC), Yokosuka, Japan. [7]Department of Evolutionary Biology and Environmental Studies, University of Zurich, Zurich, Switzerland.
*Corresponding author. Email: jskug@postech.ac.kr

RESULTS AND DISCUSSION

Seasonal and interannual fire activity over southeastern Siberia

Boreal fires usually occur in the summer because fires at high latitudes are temperature limited over the rest of the year (*14*–*16*). Central and eastern Siberian fires north of 55°N reach a maximum in June and July, but southeastern Siberian fire activity shows a monthly maximum in the spring (fig. S1) (*15*, *16*). Seasonal fire variation in southeastern Siberia peaks in both spring and autumn, but the spring peak is approximately four times greater than the autumn peak (Fig. 1B). Area burned during April and May amounts to 62% of the annual total, whereas that during September to November amounts to only 16%. Unlike northern Siberia, southeastern Siberia has noticeable summer precipitation affected by the East Asian monsoon, which suppresses summertime fire activity (fig. S2).

In addition to seasonality, southeastern Siberian fire activity also has considerable year-to-year fluctuations (Fig. 1B and fig. S3). Year-to-year fire activity has been found to be closely related to the AO index in late winter (Table 1), which is the predominant Northern Hemisphere atmospheric circulation pattern. The correlation coefficient between southeastern Siberia's annual total burned area and the February to March averaged AO index is 0.53, which is significant at the 95% confidence level. The AO is characterized by a dipole pressure pattern with one sign in the Arctic and the opposite sign in mid-latitudes (*17*). The AO is known to have enormous influence on Eurasian climate variability, affecting surface temperature, rainfall, snowfall, storm activity, and even vegetation activity (*18*–*20*). Mean burned area amounts categorized by the AO show generally greater fire activity in the higher rank bin (Fig. 1C). In particular, it is evident that the strong fire activity hardly occurs under the negative phase of the AO, and the fire activity in April is even smaller than the activity in May (Fig. 1B). Although summer AO variability is known to drive boreal fire activity simultaneously (*9*, *12*), we have found notable lagged linkage between the winter AO and spring fire activity, with strong implication on fire prediction.

Large-scale atmospheric circulation related to fire activity

Figure 2 shows low-level atmospheric circulation relative to total annual burned area in southeastern Siberia. Although April and

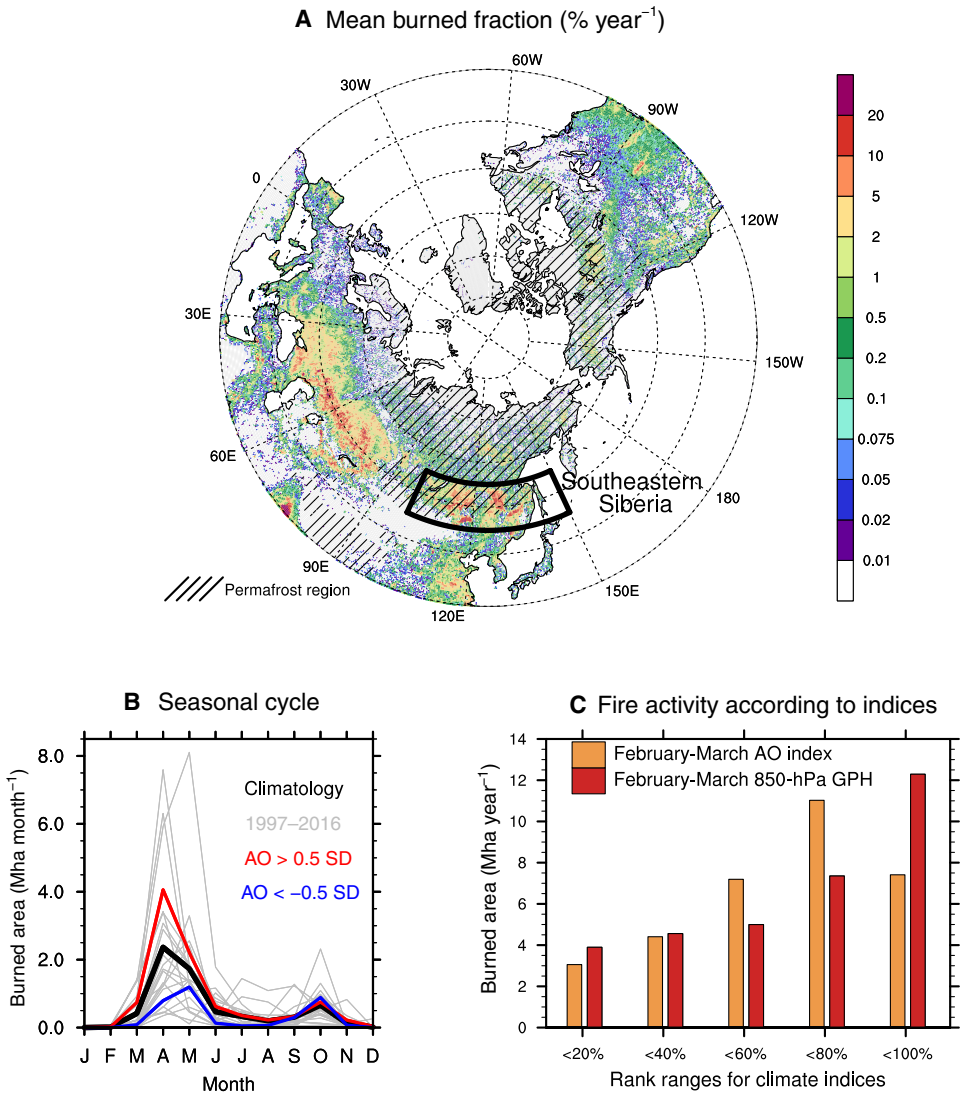

Fig. 1. Fire activity over southeastern Siberia. (**A**) Mean burned area fraction (% year^{-1}) over mid- and high latitudes in the Northern Hemisphere. Hatched areas indicate permafrost regions. The black box indicates the study area in southeastern Siberia (100°–150°E, 45°–55°N). (**B**) Monthly burned area (Mha month^{-1}) in southeastern Siberia for 1997–2016 in each year (gray), mean (thick black), composite for February to March AO index > 0.5 SD cases (red), and AO < −0.5 SD cases (blue). (**C**) Mean burned area according to February to March AO index (orange) and 850-hPa geopotential height anomaly over southeastern Siberia (red). Bins on the *x* axis indicate <20%, <40%, <60%, <80%, and <100% rank ranges.

May are peak southeastern Siberian fire activity months as shown in Fig. 1B, atmospheric circulation anomalies during those months are relatively weaker than late winter (February to March) anomalies. However, in late winter, there are distinctive negative geopotential height anomalies in the Arctic, but positive anomalies over Siberia (Fig. 2, A and B). The pressure gradient with the geopotential height pattern leads to southwesterly winds occurring in Siberia, which are accompanied by atmospheric warm advection that contributes to substantial positive temperature anomalies in Siberia during late winter. This large-scale atmospheric circulation and temperature response is similar to the AO pattern during the positive phase, with low pressure in the Arctic and high pressure in mid-latitudes (fig. S4). Strictly speaking, the fire activity–related high-pressure pattern extends further into southeastern Siberia than the typical AO pattern. This suggests that the AO provides preferable conditions for strong fire activity (i.e., high-temperature anomalies), but the positive pressure anomaly extending westward from the North Pacific to southeastern Siberia explains more southeastern Siberian fire activity variability.

As shown in Fig. 2, burned area in southeastern Siberia is closely related to local geopotential height anomalies on an interannual time scale. We define the local geopotential height index by averaging geopotential height anomalies for February and March over an area (110°–140°E, 45°–55°N) covering most of southeastern Siberia except for the eastern coastal region and the ocean. The geopotential height index highly correlates with fire activity, with a correlation coefficient of 0.80 that is significant at the 99% confidence level (fig. S5). Figure 1C shows that the local geopotential height anomaly, rather

than the AO index, is linearly proportional to fire activity. When the geopotential height is extremely high (more than 20%), the mean burned area is 1.9 times greater than the climatological value.

We found that atmospheric circulations are much stronger before the fire-active season (February to March) than in the fire-active season (April to May), as shown in Fig. 2. The AO and local geopotential height indices for February and March show significant correlations with burned area in southeastern Siberia, but not for April and May (Table 1). Local temperature and geopotential height both show positive anomalies in April, which is when southeastern Siberian burned area is at its maximum; however, these anomalies are relatively weaker than those in late winter (February to March) and are also nonsignificant (Fig. 2C). In addition, substantial land-surface cooling is observed in May over Siberia (Fig. 2D), whereas strong warming precedes strong fire activity. It is conceived that fire-induced aerosols might block solar radiation, resulting in surface cooling, suggesting that fire is largely controlled by climate factors while, in turn, considerably affecting the climate system on a seasonal time scale (*21*). An aerosol optical depth at 550 nm over northeastern Siberia (120°–180°E, 55°–70°N), where the cooling is distinctively observed, shows a significant relationship with the burned area in southeastern Siberia in May, indicating that aerosols from the southeastern Siberian fire are transported northward (table S1).

Role of earlier snowmelt on fire activity

In late winter, anticyclonic circulation accompanies anomalous southwesterlies, leading to surface warming due to warm advection over southeastern Siberia. Surface warming alters local snow conditions,

Table 1. Correlation matrix between burned area and climatic variables. * and ** indicate significance at the 95 and 99% confidence level based on Student's *t* test, respectively.

	January	February	March	April	May	June
Niño 3.4	0.13	0.14	0.13	0.11	0.06	0.10
AO	0.10	0.43	0.46*	−0.07	0.16	−0.08
850-hPa geopotential height	0.06	0.60**	0.77**	0.21	0.11	0.09
Temperature	0.08	0.41	0.54*	0.46*	−0.37	−0.19
Precipitation	−0.18	−0.40	−0.32	−0.27	−0.14	−0.08
Potential evapotranspiration	0.14	0.28	0.56**	0.50*	−0.08	−0.11

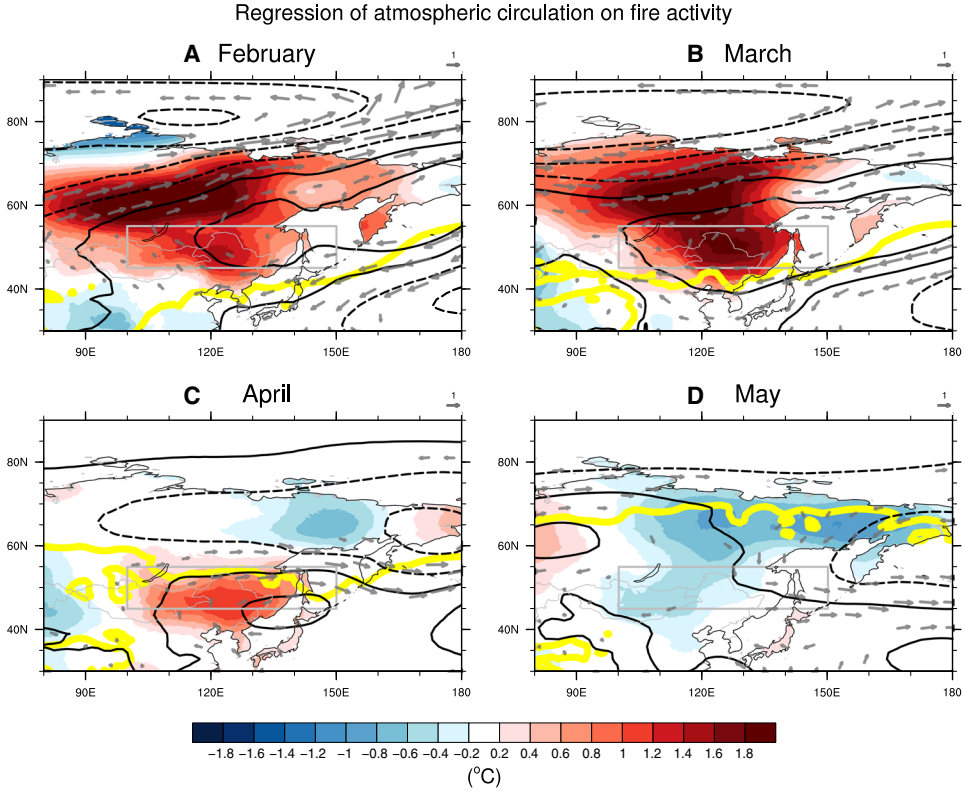

Fig. 2. Atmospheric circulation related to fire activity in southeastern Siberia. Regression coefficients of temperature (shading), 850-hPa geopotential height (contour; 100-gpm interval), and 850-hPa wind (vector) for February (**A**), March (**B**), April (**C**), and May (**D**) on normalized yearly burned area in southeastern Siberia (boxed area). The climatological 0°C line for 2-m temperature is shown as a thick yellow line. Wind vectors are displayed only in regions significant at the 95% confidence level based on Student's *t* test.

leading to an earlier start of the fire season, and is thus a preferable condition for strong fire activity. However, as shown in Fig. 2, despite notable positive temperature anomalies, southeastern Siberia has a subzero climatological temperature in late winter (Fig. 2, A and B). In addition, climatological snow cover exceeds 50% in this region, which suppresses winter fire activity (Fig. 3A). Although this region experiences notable positive temperature anomalies from February onward, February snow variability is not sensitive to temperature anomalies because the climatological temperature is too low to induce snowmelt (fig. S2). In contrast, we found a significant negative relationship between March to April snow cover and total annual fire activity, as positive temperature anomalies related to a positive AO in February and March drive early snowmelt in March and April with a time lag of 1 to 2 months (Fig. 3, B and C, and fig. S6) (*18*, *19*). This is consistent with results from a snow water equivalent dataset (fig. S7). Accumulated positive temperature anomalies in late winter lead to earlier melting in snow cover's seasonal evolution. Once snow cover is reduced, a positive snow-albedo feedback accelerates surface warming and snowmelt (fig. S8). Thus, significant negative snowmelt is observed in March and April as a result (Fig. 3, B and C). Earlier snowmelt leads to faster exposure of the ground surface and litter, which, in turn, allows favorable conditions for fire spreading because this region consists mostly of larch (*Larix gmelinii*) forests with a high amount of litter that can act as fire fuel (*22*). This seasonal response of snow cover may explain the lagged relationship between fire activity, which has its maximum in April and May, and late winter atmospheric circulation anomalies.

Fire activity related to aridity

In addition to faster ground exposure, earlier snowmelt has also been reported to lead to dry air conditions and more fires in the western United States (*23*). In southeastern Siberia, substantial late winter positive temperature anomalies not only drive earlier snowmelt but also enhance potential evaporation from the ground to the atmosphere, suggesting that the late winter's AO-like large-scale atmospheric circulation leads to dry springtime land-surface conditions (Table 1). To support this argument, we analyze each gridded ($0.5° \times 0.5°$) burned area in southeastern Siberia with respect to the aridity index, which is the ratio of precipitation to potential evapotranspiration (P/PET) (Fig. 4A). This analysis shows a generally negative relation between burned area and P/PET, meaning that more arid regions have stronger fire activity. In addition, the 850-hPa geopotential height anomaly, which explains southeastern Siberian fire activity (Fig. 1C), has a close relation to dry conditions, especially east of Lake Baikal, northeast China, and the far southeastern part of Russia (Fig. 4B). The relationship between precipitation anomalies and fire activity in March and April is not significant; therefore, increased PET is mainly induced by positive temperature anomalies as shown in Fig. 2 (Table 1). In addition, different soil moisture datasets show significant negative anomalies with respect to the 850-hPa geopotential height anomaly and AO index in April and May (fig. S9). Earlier snowmelt induces meltwater, but this meltwater cannot supply soil moisture because of the frozen soil (*24*). Unabsorbed meltwater thus runs off and evaporates due to higher atmospheric demand as a result of positive temperature

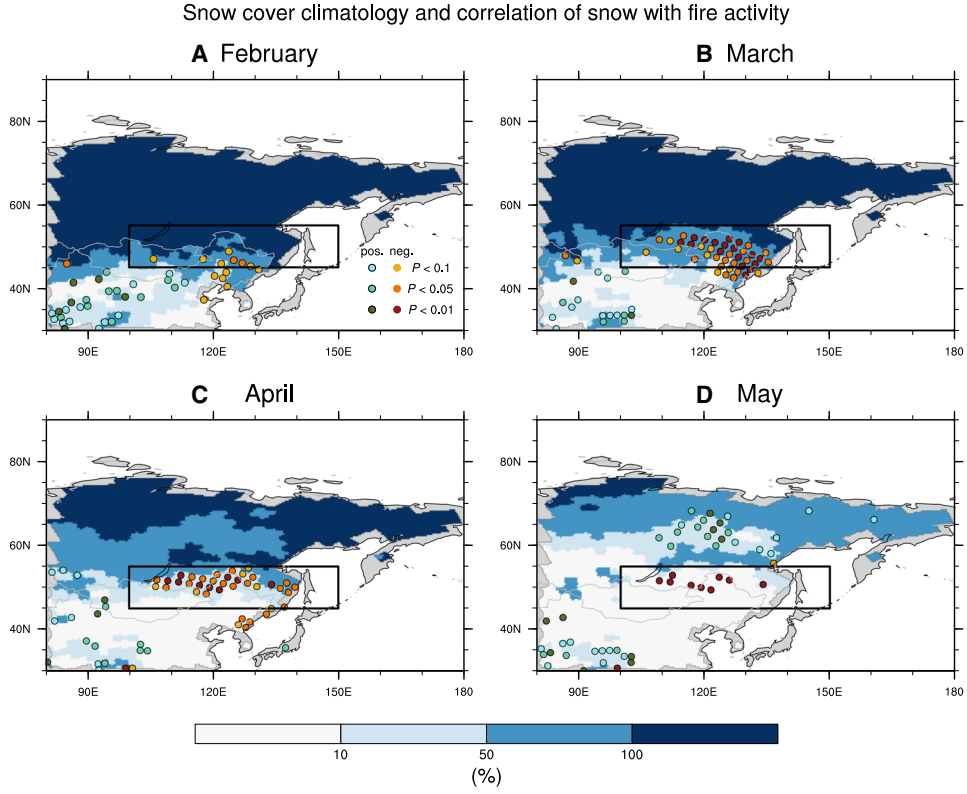

Fig. 3. Snow cover variation related to fire activity over southeastern Siberia. Climatological monthly snow cover (shading) and statistical confidence (dots) based on correlation coefficient between yearly burned area in southeastern Siberia (boxed area) and monthly snow cover anomalies for February (**A**), March (**B**), April (**C**), and May (**D**) based on Student's *t* test.

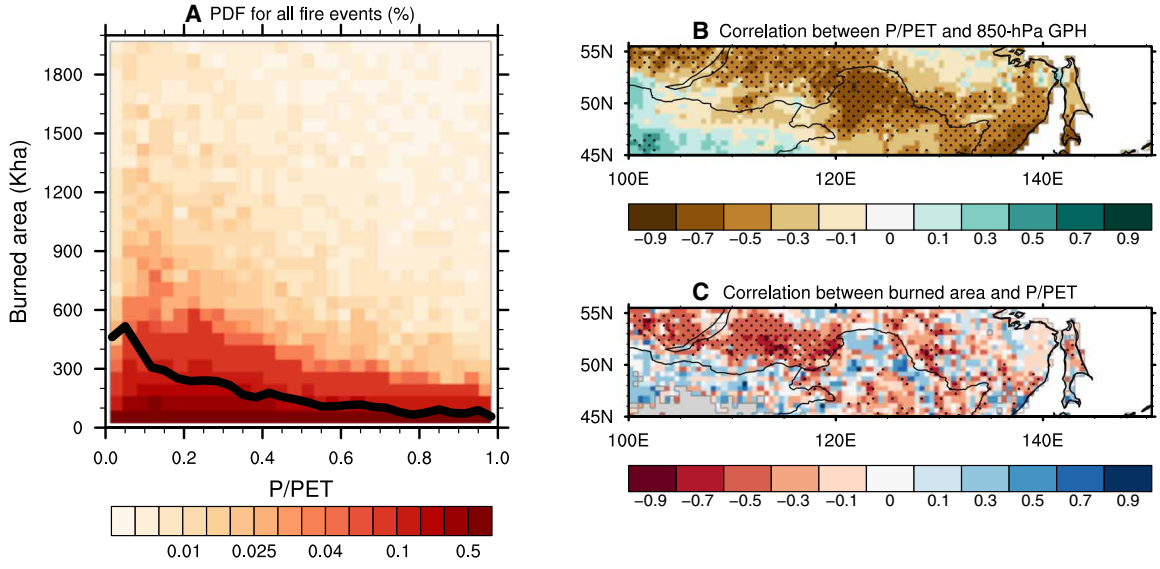

Fig. 4. Fire activity related to aridity. (**A**) Probability density function (%) for monthly precipitation to potential evapotranspiration ratio (P/PET) versus monthly regridded burned area (Kha) for each 0.5° × 0.5° grid in southeastern Siberia. The thick black line shows averaged burned area (Kha) in each P/PET bin. (**B**) Correlation coefficient map for averaged January to May P/PET with February to March 850-hPa geopotential height anomalies over southeastern Siberia. (**C**) Correlation coefficient map for total annual local burned area with January to May P/PET in each grid cell. Dotted area indicates significant region at the 90% confidence level based on Student's *t* test.

anomalies. We found that soil moisture depletion in response to temperature increase is stronger in permafrost region than in non-permafrost region (Table 2), strongly supporting our argument. However, soil moisture anomalies are not much sensitive to precipitation, suggesting that temperature anomalies related to large-scale atmospheric circulation change drive soil moisture anomalies over southeastern Siberia in late winter and early spring.

In conclusion, late winter temperature increases related to large-scale atmospheric circulation anomalies promote earlier snowmelt and drier air conditions with a time delay. This thereby increases spring fire activity chances even in the temperature-limited boreal forest area. The permafrost region is usually considered a temperature-limited region for fire regimes, and temperature is known as a primary precursor of fire activity. However, our results suggest that fire activity is not only determined by large-scale atmospheric conditions but also affected by land-atmosphere interactions, such as snowmelt, soil moisture, and aridity, which need to be considered for improving understanding of fire dynamics in southeastern Siberia.

Although large-scale atmospheric circulation overwhelms climatic conditions in most of southeastern Siberia, gridded fire records vary by region and do not show consistent features (Fig. 4C). For example, northeast China's aridity index has a significant negative relationship with the geopotential height anomaly, but this region's local burned area amount is considerably lower than that east of Lake Baikal in Russia. As shown in Fig. 1A, there are also distinct differences in the climatological burned area fraction for these regions, with northeast China having lower fire activity than southeastern Russia. It has been reported that eastern Russia experienced record-breaking fires in 2003, whereas northeast China had relatively weak fire activity at that time even though both regions had similar anomalous climatic conditions (*25*). This suggests that national forests and fire management strategy might also be critical for fire activity distribution.

In contrast to the North American boreal fires (*10*, *26*), lightning explains less than 13% of fire ignition; however, anthropogenic activity causes ignition in more than 50% of fires in southeastern Siberia (*27*–*29*). Large-scale atmospheric circulation can aggravate fire spreading, but anthropogenic activity plays a substantial role in the ignition of fires in southeastern Siberia. Temperature increases, earlier snowmelt, and dry conditions also enhance fire spreading; however, they may not contribute to ignition. Fires in intact forests in Russia have been reported to be mostly within 10 km of non-intact forest, implying anthropogenic ignition outside of intact forests (*27*). In addition, ignition mostly happens randomly due to natural causes or human activity, and fire spread is strongly controlled by climate factors; however, fire damage can be largely reduced by human fire management. Therefore, southeastern Siberia needs appropriate policies for suppressing human-driven ignition. Our findings would be useful for predictions of fire activity prediction and provide local citizens warnings to prevent socioeconomic losses and damage, as there is a time lag of 1 to 2 months between large-scale atmospheric circulation anomalies and fire activity. When a pattern conducive to strong wildfire activity is observed in late winter, vigorous fire prevention management would likely reduce fire damage considerably.

On the other hand, historical fire statistics in Russia and China show a positive fire activity trend in southeastern Siberia over the past few decades, and anthropogenic activity might contribute to this trend (fig. S3) (*30*). In addition, this region has experienced long-term spring warming (*31*) and earlier snowmelt (*32*, *33*) due to Arctic warming. Furthermore, previous studies have warned that greenhouse gas warming would enhance fire occurrence probability because of reduced relative humidity due to increased temperature (*6*, *34*). Although we only analyzed interannual variation of fire activity in southeastern Siberia, long-term climate change in this region may modulate long-term fire activity. For example, on-going regional warming and snow retreat, particularly during the winter-to-spring transition period (fig. S10), would drive more fire activity in southeastern Siberia in the near future. Therefore, on the basis of our

Table 2. Soil moisture anomalies during high-temperature case (highest 5 years) and low-precipitation case (lowest 5 years) events depending on permafrost types. * indicates significance at the 95% confidence level based on the bootstrap method. In the bootstrap method, to get probabilistic density function, random resampling is repeated 10,000 times from the observed data.

April soil moisture anomaly (m^2 m^{-2})	Continuous and discontinuous permafrost (>50%)	Sporadic permafrost (10–50%)	Isolated permafrost (0–10%)	Nonpermafrost
Composite of February to March high-temperature case	-6.83×10^{-3} ($P = 0.05$*)	-8.25×10^{-3} ($P = 0.04$*)	-8.54×10^{-3} ($P = 0.06$)	-3.27×10^{-3} ($P = 0.19$)
Composite of February to March low-precipitation case	-0.38×10^{-3} ($P = 0.49$)	-4.53×10^{-3} ($P = 0.16$)	-1.19×10^{-3} ($P = 0.37$)	-0.39×10^{-3} ($P = 0.45$)

findings, a lengthening of snow-free days and fire season according to ongoing pan-Arctic warming must be considered for predicting long-term fire activity and establishing fire management policies. Despite the importance of long-term fire projections, current Earth system models tend to underestimate boreal fire activity (*35*). In addition, it is also possible that boreal fires accelerate permafrost thaw through deepening of the active layer (*36*). As boreal fires play a considerable carbon-climate feedback role because of peatlands' high-level carbon emissions, precise fire modeling is needed for accurate future projection of pan-Arctic climate change and the global carbon budget.

MATERIALS AND METHODS

Dataset

We used data from GFED4.1s for the period 1997–2016 (https://www.globalfiredata.org/) to obtain fire burned area in the pan-Arctic and southeastern Siberia regions (*4*). The monthly AO index was downloaded from Climate Prediction Center (https://www.cpc.ncep.noaa.gov/products/precip/CWlink/daily_ao_index/ao_index.html). To estimate atmospheric circulation patterns related to fire activity, we obtained monthly geopotential height and wind data in 1.5° × 1.5° resolution from the European Centre for Medium-Range Weather Forecasts Reanalysis-Interim (http://apps.ecmwf.int/datasets/) (*37*). We quantified monthly surface temperature, precipitation, and potential evapotranspiration in 0.5° × 0.5° resolution using Climatic Research Unit TS4.01 (http://www.cru.uea.ac.uk) (*38*). Monthly snow cover data are from Rutgers University Climate Laboratory (http://climate.rutgers.edu/snowcover) (*39*).

Linear regression analysis

To reveal the fire activity–related large-scale atmospheric conditions, we performed a linear regression analysis to normalized yearly burned area in southeastern Siberia based on GFED4.1s for the period 1997–2016. The significance test conducted in this study is based on the standard two-tailed Student's *t* test.

SUPPLEMENTARY MATERIALS

Supplementary material for this article is available at http://advances.sciencemag.org/cgi/content/full/6/2/eaax3308/DC1

Table S1. Correlation matrix between burned area and aerosol optical depth at 550 nm based on MISR.
Fig. S1. Month of maximum of fire activity.
Fig. S2. Temperature and precipitation climatology.
Fig. S3. Interannual variability of fire activity.
Fig. S4. Atmospheric circulation related to AO index.
Fig. S5. Climate indices versus burned area over southeastern Siberia.
Fig. S6. Snow cover variation related to AO.
Fig. S7. Snow water equivalent variation related to fire activity over southeastern Siberia.
Fig. S8. Fire activity–related snow-albedo feedback term.
Fig. S9. Soil moisture anomalies related to 850-hPa geopotential height anomaly and AO index.
Fig. S10. Snow cover trend.
References (*40*–*44*)

REFERENCES AND NOTES

1. E. G. Jobbagy, R. B. Jackson, The vertical distribution of soil organic carbon and its relation to climate and vegetation. *Ecol. Appl.* **10**, 423–436 (2000).
2. E. A. G. Schuur, A. D. McGuire, C. Schädel, G. Grosse, J. W. Harden, D. J. Hayes, G. Hugelius, C. D. Koven, P. Kuhry, D. M. Lawrence, S. M. Natali, D. Olefeldt, V. E. Romanovsky, K. Schaefer, M. R. Turetsky, C. C. Treat, J. E. Vonk, Climate change and the permafrost carbon feedback. *Nature* **520**, 171–179 (2015).
3. S.-J. Jeong, A. A. Bloom, D. Schimel, C. Sweeney, N. C. Parazoo, D. Medvigy, G. Schaepman-Strub, C. Zheng, C. R. Schwalm, D. N. Huntzinger, A. M. Michalak, C. E. Miller, Accelerating rates of Arctic carbon cycling revealed by long-term atmospheric CO_2 measurements. *Sci. Adv.* **4**, eaao1167 (2018).
4. G. R. van der Werf, J. T. Randerson, L. Giglio, T. T. van Leeuwen, Y. Chen, B. M. Rogers, M. Mu, M. J. E. van Marle, D. C. Morton, G. J. Collatz, R. J. Yokelson, R. S. Kasibhatla, Global fire emissions estimates during 1997–2016. *Earth Syst. Sci. Data* **9**, 679–720 (2017).
5. M. C. Mack, M. S. Bret-Harte, T. N. Hollingsworth, R. R. Jandt, E. A. G. Schuur, G. R. Shaver, D. L. Verbyla, Carbon loss from an unprecedented Arctic tundra wildfire. *Nature* **475**, 489–492 (2011).
6. M. R. Turetsky, B. Benscoter, S. Page, G. Rein, G. R. van der Werf, A. Watts, Global vulnerability of peatlands to fire and carbon loss. *Nat. Geosci.* **8**, 11–14 (2015).
7. J. T. Randerson, Y. Chen, G. R. van der Werf, B. M. Rogers, D. C. Morton, Global burned area and biomass burning emissions from small fires. *J. Geophys. Res.* **117**, G04012 (2012).
8. C. Warneke, R. Bahreini, J. Brioude, C. A. Brock, J. A. de Gouw, D. W. Fahey, K. D. Froyd, J. S. Holloway, A. Middlebrook, L. Miller, S. Montzka, D. M. Murphy, J. Peischl, T. B. Ryerson, J. P. Schwarz, J. R. Spackman, P. Veres, Biomass burning in Siberia and Kazakhstan as an important source for haze over the Alaskan Arctic in April 2008. *Earth Syst. Sci. Lett.* **36**, L02813 (2009).
9. H. Balzter, F. F. Gerard, C. T. George, C. S. Rowland, T. E. Jupp, I. McCallum, A. Shvidenko, S. Nilsson, A. Sukhinin, A. Onuchin, C. Schmullius, Impact of the Arctic Oscillation pattern on interannual forest fire variability in central Siberia. *Geophys. Res. Lett.* **32**, L14709 (2005).
10. M. Macias Fauria, E. A. Johnson, Large-scale climatic patterns control large lightning fire occurrence in Canada and Alaska forest regions. *J. Geophys. Res.* **111**, G04008 (2006).
11. W. R. Skinner, A. Shabbar, M. D. Flannigan, K. Logan, Large forest fires in Canada and the relationship to global sea surface temperatures. *J. Geophys. Res.* **111**, D14106 (2006).
12. H. Balzter, F. Gerard, C. George, G. Weedon, W. Grey, B. Combal, E. Bartholomé, S. Bartalev, S. Los, Coupling of vegetation growing season anomalies and fire activity with hemispheric and regional-scale climate patterns in central and east Siberia. *J. Climate* **20**, 3713–3729 (2007).
13. M. Macias Fauria, E. A. Johnson, Climate and wildfires in the North American boreal forest. *Phil. Trans. R. Soc. B* **363**, 2317–2329 (2008).
14. A. J. Soja, W. R. Cofer, H. H. Shugart, A. I. Sukhinin, P. W. Stackhouse Jr., D. J. McRae, S. G. Conard, Estimating fire emissions and disparities in boreal Siberia (1998–2002). *J. Geophys. Res.* **109**, D14S06 (2004).

15. A. J. Soja, A. I. Sukhinin, D. R. Cahoon Jr., H. H. Shugart, P. W. Stackhouse Jr., AVHRR-derived fire frequency, distribution and area burned in Siberia. *Int. J. Remote Sens.* **25**, 1939–1960 (2004).
16. E. I. Ponomarev, V. I. Kharuk, K. J. Ranson, Wildfires dynamics in Siberian larch forests. *Forests* **7**, 125 (2016).
17. D. W. Thompson, J. M. Wallace, The Arctic Oscillation signature in the wintertime geopotential height and temperature fields. *Geophys. Res. Lett.* **25**, 1297–1300 (1998).
18. A. S. Bamzai, Relationship between snow cover variability and Arctic Oscillation index on a hierarchy of time scales. *Int. J. Climatol.* **23**, 131–142 (2003).
19. K. Schaefer, S. Denning, O. Leonard, The winter Arctic Oscillation, the timing of spring, and carbon fluxes in the Northern Hemisphere. *Global Biogeochem. Cycles* **19**, GB3017 (2005).
20. M.-H. Cho, G.-H. Lim, H.-J. Song, The effect of the wintertime Arctic Oscillation on springtime vegetation over the northern high latitude region. *Asia-Pac. J. Atmos. Sci.* **50**, 567–573 (2014).
21. A. Stohl, Characteristics of atmospheric transport into the Arctic troposphere. *J. Geophys. Res.* **111**, D11306 (2006).
22. B. M. Rogers, A. J. Soja, M. L. Goulden, J. T. Randerson, Influence of tree species on continental differences in boreal fires and climate feedbacks. *Nat. Geosci.* **8**, 228–234 (2015).
23. A. L. Westerling, H. G. Hidalgo, C. D. Cayan, T. W. Swetnam, Warming and earlier spring increase western U.S. forest wildfire activity. *Science* **313**, 940–943 (2006).
24. M. Forkel, K. Thonicke, C. Beer, W. Cramer, S. Bartalev, C. Schmullius, Extreme fire events are related to previous-year surface moisture conditions in permafrost-underlain larch forests of Siberia. *Environ. Res. Lett.* **7**, 044021 (2012).
25. S. Huang, F. Siegert, J. G. Goldammer, A. I. Sukhinin, Satellite-derived 2003 wildfires in southern Siberia and their potential influence on carbon sequestration. *Int. J. Remote Sens.* **30**, 1479–1492 (2009).
26. S. Veraverbeke, B. M. Rogers, M. L. Goulden, R. R. Jandt, C. E. Miller, E. B. Wiggins, J. T. Randerson, Lightning as a major driver of recent large fire years in North American boreal forests. *Nat. Clim. Change* **7**, 529–534 (2017).
27. D. Mollicone, H. D. Eva, F. Achard, Human role in Russian wild fires. *Nature* **440**, 436–437 (2006).
28. F. Archard, H. D. Eva, D. Mollicone, R. Beuchle, The effect of climate anomalies and human ignition factor on wildfires in Russian boreal forests. *Philos. Trans. R. Soc. B* **363**, 2331–2339 (2008).
29. E. A. Kukavskaya, L. V. Buryak, E. G. Shvetsov, S. G. Conard, O. P. Kalenskaya, The impact of increasing fire frequency on forest transformations in southern Siberia. *For. Ecol. Manage.* **382**, 225–235 (2016).
30. Y. Zhang, D. Qin, W. Yuan, B. Jia, Historical trends of forest fires and carbon emissions in China from 1988 to 2012. *J. Geophys. Res.* **121**, 2506–2517 (2016).
31. J. L. Cohen, J. C. Furtado, M. Barlow, V. A. Alexeev, J. E. Cherry, Asymmetric seasonal temperature trends. *Geophys. Res. Lett.* **39**, L04705 (2012).
32. H. Park, A. N. Fedorov, M. N. Zheleznyak, P. Y. Konstantinov, J. E. Walsh, Effect of snow cover on pan-Arctic permafrost thermal regimes. *Climate Dynam.* **44**, 2873–2895 (2015).
33. R. Brown, C. Derksen, L. Wang, A multi-data set analysis of variability and change in Arctic spring snow cover extent, 1967–2008. *J. Geophys. Res.* **115**, D16111 (2010).
34. N. M. Tchebakova, E. Parfenova, A. J. Soja, The effects of climate, permafrost and fire on vegetation change in Siberia in a changing climate. *Environ. Res. Lett.* **4**, 045013 (2009).
35. C. Yue, P. Ciais, D. Zhu, T. Wang, S. S. Peng, S. L. Piao, How have past fire disturbances contributed to the current carbon balance of boreal ecosystems? *Biogeosciences* **13**, 675–690 (2016).
36. C. M. Gibson, L. E. Chasmer, D. K. Thompson, W. L. Quinton, M. D. Flannigan, D. Olefeldt, Wildfire as a major driver of recent permafrost thaw in boreal peatlands. *Nat. Commun.* **9**, 3041 (2018).
37. D. P. Dee, S. M. Uppala, A. J. Simmons, P. Berrisford, P. Poli, S. Kobayashi, U. Andrae, M. A. Balmaseda, G. Balsamo, P. Bauer, P. Bechtold, A. C. M. Beljaars, L. van de Berg, J. Bidlot, N. Bormann, C. Delsol, R. Dragani, M. Fuentes, A. J. Geer, L. Haimberger, S. B. Healy, H. Hersbach, E. V. Hólm, L. Isaksen, P. Kållberg, M. Köhler, M. Matricardi, A. P. McNally, B. M. Monge-Sanz, J.-J. Morcrette, B.-K. Park, C. Peubey, P. de Rosnay, C. Tavolato, J.-N. Thépaut, F. Vitart, The ERA-Interim reanalysis: Configuration and performance of the data assimilation system. *Q. J. R. Meteorol. Soc.* **137**, 553–597 (2011).
38. I. Harris, P. D. Jones, T. L. Osborn, D. H. Lister, Updated high-resolution grids of monthly climatic observations – the CRU TS3.10 Dataset. *Int. J. Climatol.* **34**, 623–642 (2014).
39. T. W. Estilow, A. H. Young, D. A. Robinson, A long-term Northern Hemisphere snow cover extent data record for climate studies and monitoring. *Earth Syst. Sci. Data* **7**, 137–142 (2015).
40. M. K. Takala, K. Luojus, J. Pulliainen, C. Derksen, J. Lemmetyinen, J.-P. Kärnä, J. Koskinen, B. Bojkov, Estimating northern hemisphere snow water equivalent for climate research through assimilation of space--borne radiometer data and ground-based measurements. *Remote Sens. Environ.* **115**, 3517–3529 (2011).
41. R. A. Kahn, B. J. Gaitley, M. J. Garay, D. J. Diner, T. F. Eck, A. Smirnov, B. N. Holben, Multiangle Imaging SpectroRadiometer global aerosol product assessment by comparison with the Aerosol Robotic Network. *J. Geophys. Res. Atmos.* **115**, D23209 (2010).
42. K. M. Shell, J. T. Kiehl, C. A. Shields, Using the radiative kernel technique to calculate climate feedbacks in NCAR's Community Atmospheric Model. *J. Climate* **21**, 2269–2282 (2008).
43. B. Martens, GLEAMv3: Satellite-based land evaporation and root-zone soil moisture. *Geosci. Model Dev.* **10**, 1903–1925 (2017).
44. Y. Fan, H. M. van den Dool, Climate prediction center global monthly soil moisture data set at 0.5° resolution for 1948 to present. *J. Geophys. Res.* **109**, D10102 (2004).

Acknowledgments

Funding: This research was supported under the framework of International Cooperation Programme, Young Researchers Exchange Programme between Korea and Switzerland, managed by the National Research Foundation of Korea (NRF-2016K1A3A1A14952989). J.-S.Ki. was additionally supported by the Natural Environment Research Council of United Kingdom through the National Centre for Earth Observation. J.-S.Ku. was supported by the National Research Foundation of Korea (NRF-2018R1A5A1024958). S.-J.J. was supported by Korea Environment Industry and Technology Institute (KEITI) through Public Technology Program based on Environmental Policy Program, funded by the Korea Ministry of Environment (MOE) (2019000160007) and the Korea Meteorological Administration Research and Development Program under Grant KMI (KMI2018-03711). H.P. was supported by the Japan Agency for Marine-Earth Science and Technology (JAMSTEC). G.S.-S. was supported by University of Zurich Research Priority Programme "Global Change and Biodiversity" (URPP GCB). **Author contributions:** J.-S.Ki. compiled the data, conducted analyses, prepared figures, and wrote the manuscript. J.-S.Ku., S.-J.J., H.P., and G.S.-S. designed the research and wrote the majority of the manuscript content. All the authors discussed the study results and reviewed the manuscript. **Competing interests:** The authors declare that they have no competing interests. **Data and materials availability:** All data needed to evaluate the conclusions in the paper are present in the paper and/or the Supplementary Materials. Additional data related to this paper may be requested from the authors.

Submitted 14 March 2019
Accepted 7 November 2019
Published 8 January 2020
10.1126/sciadv.aax3308

Citation: J.-S. Kim, J.-S. Kug, S.-J. Jeong, H. Park, G. Schaepman-Strub, Extensive fires in southeastern Siberian permafrost linked to preceding Arctic Oscillation. *Sci. Adv.* **6**, eaax3308 (2020).